Biochemical Pharmacology 78 (2009) 1382–1390

Contents lists available at ScienceDirect

Biochemical Pharmacology

journal homepage: www.elsevier.com/locate/biochempharm

Photolabeling identifies transmembrane domain 4 of CXCR4 as a T140 binding site

Philip E. Boulais [a], Dominic Dulude [b,c], Jérôme Cabana [a], Nikolaus Heveker [b,c], Emanuel Escher [a], Pierre Lavigne [a], Richard Leduc [a,*]

[a] Department of Pharmacology, Faculty of Medicine and Health Sciences, Université de Sherbrooke, Sherbrooke, Québec, Canada J1H5N4
[b] Department of Biochemistry, Université de Montréal, Montréal, Québec, Canada H3T1J4
[c] Centre de Recherche, Hôpital Sainte-Justine, Montréal, Canada H3T1C5

ARTICLE INFO

Article history:
Received 20 May 2009
Accepted 15 July 2009

Keywords:
CXCR4
T140
GPCR
Photoaffinity labeling
Molecular modeling
Ligand-binding pocket

ABSTRACT

CXCR4, a G-protein-coupled receptor, which binds the chemokine stromal cell-derived factor 1 alpha (SDF-1α, CXCL12), is one of two co-receptors most frequently used by HIV-1 to infect CD4+ lymphocytes. The SDF-1α/CXCR4 axis is also involved in angiogenesis, in stem cell homing to bone marrow, in rheumatoid arthritis and in cancer. Here, we directly determined the binding site of the inverse agonist T140 on CXCR4 using photoaffinity labeling. Two T140 photoanalogs were synthesized containing the photoreactive amino acid *p*-benzoyl-L-phenylalanine (Bpa) in positions 5 or 10, yielding [Bpa^5]T140 and [Bpa^{10}]T140. Binding experiments on HEK293 cells stably expressing the wild-type CXCR4 receptor using ^{125}I-SDF-1α demonstrated that T140 and both photoanalogs had affinities in the nanomolar range, similar to SDF-1α. Photolabeling led to the formation of specific, covalent 42 kDa T140–CXCR4 complexes. V8 protease digestion of both CXCR4/^{125}I-[Bpa^5]T140 and CXCR4/^{125}I-[Bpa^{10}]T140 adducts generated a fragment of 6 kDa suggesting that the T140 photoanalogs labeled a fragment corresponding to Lys^{154}-Glu^{179} of the receptor's 4th transmembrane domain. Further digestion of this 6 kDa fragment with endo Asp-N led to the generation of a shorter fragment validating the photolabeled region. Our results demonstrate that T140 interacts with residues of the fourth transmembrane domain of the CXCR4 receptor and provide new structural constraints enabling us to model the complex between T140 and CXCR4.

1. Introduction

Chemokines are small proteins that act as chemoattractants for various leukocyte subpopulations [1] as well as non-hematopoietic cells [2]. The chemokine superfamily is divided into four groups (CXC, CX$_3$C, CC and C) according to the position of the first two cysteines [3]. The CXC chemokine stromal cell-derived factor 1 alpha (SDF-1α, also known as CXCL12) triggers many cellular processes such as leukocyte maturation and trafficking [1], stem cell homing to bone marrow [4,5] and angiogenesis [6]. SDF-1α is also involved in rheumatoid arthritis [7] and cancer [8]. The actions of SDF-1α are mediated by CXCR4 [9], a 'class A' G-protein-coupled receptor, but also through CXCR7 [10], a newly reported SDF-1α receptor. CXCR4 is present in many types of leukocytes such as T and B lymphocytes, monocytes, neutrophils [11] and its expression is upregulated in different cancers including breast cancer [12]. The receptor is involved in promoting tumor metastasis [13] and acts as a co-receptor for HIV-1 infection of CD4$^+$ T lymphocytes [14]. The interaction of glycoprotein gp120 of HIV-1 with the CD4 receptor and co-receptor CXCR4 (or CCR5) is a critical step in the infection process [15].

The identification of CXCR4 as a major player in HIV-1 infection made it a promising target for the development of new antiretroviral drugs such as the bicyclam AMD3100 [16] and the peptidomimetic T140 [17]. T140 is a 14-residue (Arg-Arg-Nal-Cys-Tyr-Arg-Lys-DLys-Pro-Tyr-Arg-Cit-Cys-Arg) synthetic peptide based on the primary structure of a polyphemusin peptide isolated from horseshoe crab developed through structure–activity studies by the group of Fujii [18]. T140 and analogs have inhibitory properties towards HIV-1 infection [19], rheumatoid arthritis [20] and the progression of metastasis in breast cancer [21]. T140 was originally described as a CXCR4 antagonist by virtue of its capacity to block SDF-1α binding to CXCR4. Subsequently, T140 has been found to be a CXCR4 inverse agonist by reducing basal [^{35}S]GTPγS binding to constitutively active CXCR4 receptor mutants [22].

A better understanding of the molecular basis by which T140 interacts with CXCR4 would provide new insights in the structure–activity relationship of CXCR4 and could ultimately contribute to the design of novel and/or improved antiretroviral or anti-cancer compounds. Structure–function studies based on alanine scanning

* Corresponding author. Tel.: +1 819 564 5413; fax: +1 819 564 5400.
E-mail address: Richard.Leduc@USherbrooke.ca (R. Leduc).

0006-2952/$ – see front matter © 2009 Elsevier Inc. All rights reserved.
doi:10.1016/j.bcp.2009.07.007

of the T140 primary sequence have shown that Arg^2, Nal^3, Tyr^5 and Arg^{14} are essential for anti-HIV activity [23]. Conversely, substitution mutagenesis studies on the CXCR4 receptor have revealed the importance of specific residues involved in binding SDF-1α [24,25] or the HIV envelope protein gp120 [26]. Similarly, reduced binding of [^{125}I]-T140 on CXCR4 receptors mutated at selected residues suggested that Asp^{171}, Arg^{188}, Tyr^{190}, Gly^{207} and Asp^{262} may act as key residues for the interaction of CXCR4 with T140 and were compatible with computer simulations of the receptor–ligand complex [27].

Here we use photoaffinity labeling to directly probe wild-type CXCR4 in order to identify residues that interact with T140 analogs containing the photoreactive amino acid *p*-benzoyl-L-phenylalanine (Bpa). Photoaffinity labeling using Bpa [28] has been successful for the identification of binding sites within the angiotensin II type-1 receptor [29,30], the urotensin II receptor [31], the motilin receptor [32] as well as many others. This approach allows us to identify specific residues or regions of a receptor interacting directly with Bpa thereby enabling direct mapping within a given binding pocket. Here we probed the specific interaction of ^{125}I-[Bpa^5]T140 and ^{125}I-[Bpa^{10}]T140 with CXCR4.

2. Materials and methods

2.1. Materials

Acrylamide, bovine serum albumin (BSA), deoxycholic acid, polyethylenimine and puromycin were from Sigma (Oakville, ON, Canada). Ammonium bicarbonate was from Fischer Scientific (Fair Lawn, NJ, USA). Complete protease cocktail inhibitor, endo AspN (endoproteinase Asp-N; EC 3.4.24.33), glycine, Nonidet P40, Staphylococcal V8 protease (Endo Glu-C; EC 3.4.21.19) were from Roche (Indianapolis, IN, USA). X-Omat® Blue (XB) films (Kodak), ^{125}I-SDF-1α (2200 Ci/mmol) were from PerkinElmer Life and Analytical Sciences (Woodbridge, ON, Canada). DMEM (Dulbecco's modified Eagle's medium), FBS (foetal bovine serum) and penicillin/streptomycin were obtained from Gibco Life Technologies (Gaithersburg, MD, USA). Sodium dodecyl sulfate (SDS) and sodium phosphate dibasic anhydrous (Na_2HPO_4) were from Mallinckrodt Baker, Inc. (Phillipsburg, NJ, USA). HEK293 stably expressing N-terminally HA-tagged CXCR4 was kindly provided by Dr. Michel Bouvier (Department of Biochemistry, University of Montreal, QC, Canada). Human SDF-1α was from PeproTech (Rocky Hills, NJ, USA).

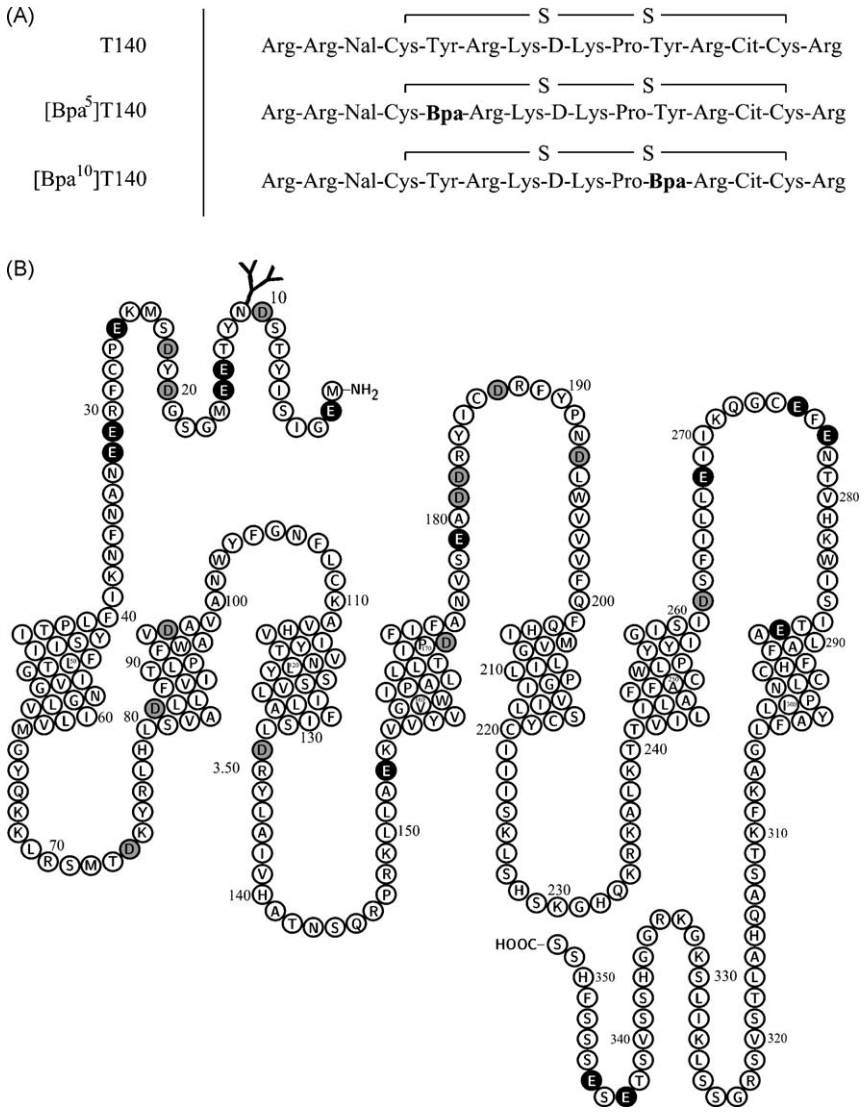

Fig. 1. (A) Amino acid sequence of T140 and T140 photoreactive analogs. Bpa residues are represented in bold. (B) Two-dimensional representation of the primary structure of human CXCR4 receptor. Black closed circles indicate cleavage sites for V8 protease. Gray closed circles indicate cleavage sites for Endo Asp-N protease.

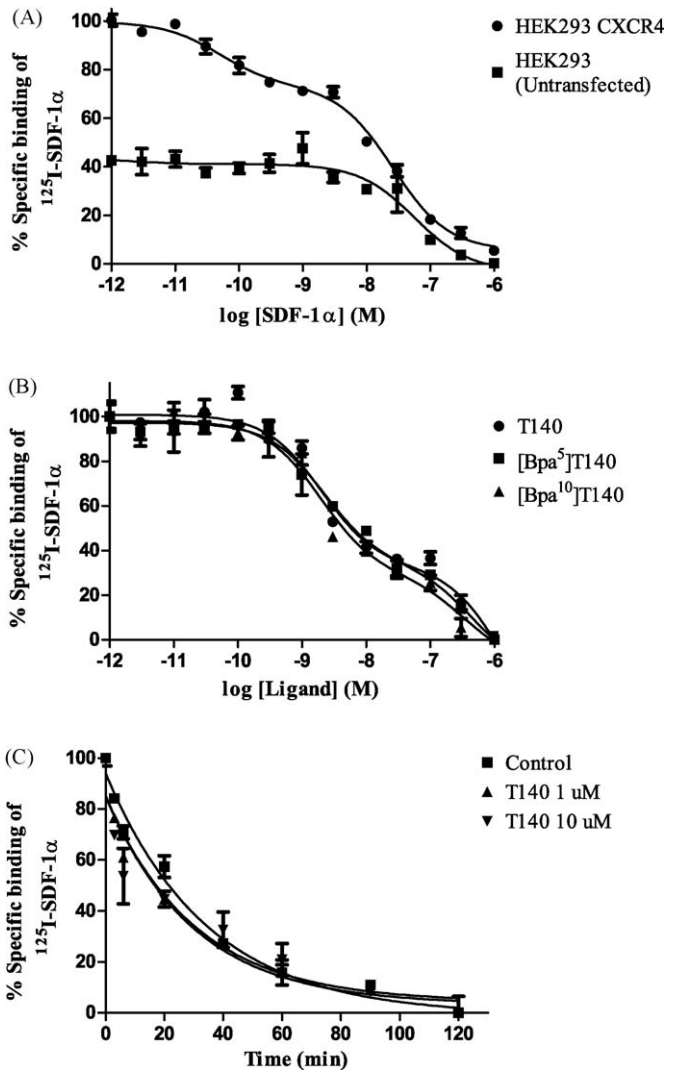

Fig. 2. Binding studies on HEK293 cells stably expressing CXCR4. (A) Competition binding using ^{125}I-SDF-1α on HEK293 stably expressing CXCR4 versus untransfected HEK293 cells. (B) Competition binding of ^{125}I-SDF-1α using T140 and the photoanalogs on HEK293 stably expressing CXCR4. These results (A, B) are representative of at least 3 separate experiments. (C) Dissociation kinetics using ^{125}I-SDF-1α on HEK293 cells stably expressing CXCR4. These results (C) are representative of 2 separate experiments. Competition studies with broken cells expressing CXCR4 were carried out as described under Section 2.4. K_i values were determined using GraphPad Prism version 5.00 for Windows.

2.2. Peptide synthesis and radioiodination

T140 and Bpa-containing T140 analogs were synthesized in our laboratories on an automatic peptide synthesis instrument (Pioneer), using the Nα-Fmoc protection strategy and TBTU (*o*-Benzotriazol-1-yl-*N*,*N*,*N*′,*N*′-tetramethyluronium tetrafluoroborate) as coupling agent, starting for each peptide with 0.3 g Fmoc Arg(Pbf)-PEG-PS resin from Novabiochem (0.22 meq/g; Gibbstown, NJ, USA). Side-chain functional groups of cysteine residues were protected by trityl groups, Arginine by Pbf (2,2,4,6,7-pentamethyldihydrobenzofuran-5-sulfonyl), Tyrosine by *t*-Butyl and Lysines by Boc which were all simultaneously removed during solid support cleavage by 92.5% aqueous trifluoroacetic acid (TFA) containing 2.5% of ethanedithiol and 2.5% triisopropylsilane. Disulfide bond formation was achieved by oxidation with DMSO. The synthetic peptides were purified to homogeneity (at least 95%) on a C_{18} reverse-phase column. Each peptide was characterized by analytical HPLC and mass spectrometry. ^{125}I-[Bpa^5]T140 and ^{125}I-[Bpa^{10}]T140 were prepared with Iodo-Gen® (1,3,4,6-tetrachloro-3α,6α-diphenylglycoluril) from Pierce Chemical Co. (Rockford, IL, USA) as described [33]. Briefly, 10 μl of a 1 mM peptide solution was incubated with 5 μg of Iodo-Gen®, 80 μl of 100 mM borate buffer, pH 8.5, and 1 mCi of Na^{125}I for 30 min at room temperature (25 °C) before being purified by HPLC on a C_{18} column.

Table 1
Binding properties of T140 analogs.

Ligand	K_i Site 1 (nM)	K_i Site 2 (nM)
SDF-1α	0.4 ± 0.4	31 ± 12
T140	2.6 ± 2.5	84 ± 36
[Bpa^5]T140	2.8 ± 0.9	40 ± 20
[Bpa^{10}]T140	1.1 ± 0.8	63 ± 8.8

HEK293 stably expressing CXCR4 were assayed as described in Section 2.4. Binding affinities (K_i) are expressed as the means ± SEM. These results were obtained in 3 independent experiments performed in triplicate.

Table 2
Inhibition of HIV infection by T140 and its analogs.

Ligand	IC_{50} (nM)	pIC_{50} ± SEM
T140	54	−7.27 ± 0.08
[Bpa^5]T140	261	−6.58 ± 0.02
[Bpa^{10}]T140	107	−6.97 ± 0.01

373-X4.15 reporter cells were infected with HIV-$1_{89.6}$ in the presence of the different compounds. Data are means ± SEM of two independent experiments performed in triplicate.

2.3. Cell culture

HEK293 cells were grown in DMEM containing 10% (v/v) FBS, 100 IU/ml penicillin and 100 μg/ml streptomycin at 37 °C. HEK293 stably expressing CXCR4 were grown using puromycin (3 μg/ml) as a selection agent. Confluent cells (95%) in 100-mm-diameter Petri dishes were used for photoaffinity labeling and binding assays.

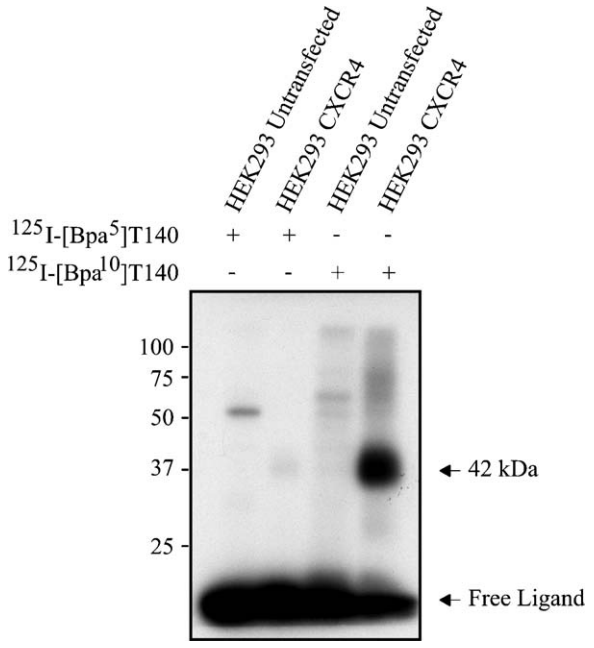

Fig. 3. Photolabeling specificity of ^{125}I-[Bpa^5]T140 or ^{125}I-[Bpa^{10}]T140. Untransfected HEK293 cells (lanes 1, 3) and HEK293 cells stably expressing CXCR4 (lanes 2, 4) were photolabeled using ^{125}I-[Bpa^5]T140 (lanes 1, 2) or ^{125}I-[Bpa^{10}]T140 (lanes 3, 4). Following photolabeling, proteins were solubilized, denatured and submitted to SDS-PAGE on 10% acrylamide gel followed by autoradiography. Protein standards of the indicated molecular masses (kDa) were run in parallel. These results are representative of at least 3 separate experiments.

2.4. Binding experiments

HEK293 cells were washed once with PBS and subjected to one freeze–thaw cycle. Broken cells were then gently scraped in binding buffer (50 mM Hepes, pH 7.4, 1 mM $CaCl_2$ and 5 mM $MgCl_2$), centrifuged at 3500 g for 15 min at 4 °C and resuspended in binding buffer containing 0.1% BSA. For competition binding assays, broken cells (1–10 μg of protein) were incubated for 1 h at room temperature in binding buffer with ^{125}I-SDF-1α (0.4 nM) as a tracer and increasing concentrations of T140 peptide analogs or SDF-1α in a final volume of 0.5 ml. Bound radioactivity was separated from free ligand by filtration through GF/C filters pre-soaked for 2 h in polyethylenimine 0.2% at 4 °C and washed with ice-cold washing buffer (50 mM Hepes, pH 7.4, 500 mM NaCl). Receptor-bound radioactivity was evaluated by γ-radiation counting. Specific binding was defined as the difference of binding in the absence and presence of 1 μM of the corresponding unlabeled ligand. Radioligand binding assays were collected in triplicate and are presented as means ± SEM. Binding curves were fitted using a binding model for two sites (R^2 = 0.9866) and K_i values were determined using GraphPad Prism version 5.00 (GraphPad Software, San Diego, CA) using non-linear regression.

Dissociation kinetic assays were performed using ^{125}I-SDF-1α (0.4 nM) in binding buffer in a final volume of 500 μl. We used the isotopic dilution method [34] to measure the dissociation rate constant for ^{125}I-SDF-1α. 1 μg of broken cells stably expressing CXCR4 were pre-incubated with ^{125}I-SDF-1α for 1 h at room temperature. Dissociation was then initiated by the addition of unlabeled SDF-1α (1 μM) in presence or absence of different concentration of T140. Dissociation times from 2 to 120 min at room temperature were used. To determine non-specific binding, dissociation experiments on broken cells by pre-incubating with ^{125}I-SDF-1α and with 1 μM SDF-1α. Bound radioactivity was then separated from free ligand by filtration through GF/C filters pre-soaked for 2 h in polyethylenimine 0.2% at 4 °C and washed with ice-cold washing buffer. Receptor-bound radioactivity was evaluated by γ-radiation counting.

2.5. HIV infection

Inhibition of HIV infection by T140 and Bpa-derivatives was measured using the reporter cell line U373-X4.15 [35], and the dualtropic HIV strain HIV-$1_{89.6}$ [36]. Infectious virus was produced from HEK293 cells transfected with HIV-$1_{89.6}$ proviral DNA (obtained from the NIH AIDS Research & Reference Reagent Program) and infection assays performed as described [24,25]. Briefly, cells were seeded in microtiter plates and cultured overnight before incubating them with various concentrations of compounds and HIV-$1_{89.6}$ for 24 h. Cells were then lysed and beta-galactosidase content measured using the colorimetric substrate CPRG (chlorophenolred-β-D-galactopyranoside).

2.6. Photoaffinity labeling

Photoaffinity labeling was performed essentially as described previously [31]. HEK293 cells stably expressing CXCR4 were incubated for 1 h at room temperature in 0.5 ml of binding buffer containing the photoreactive radioligand (50 nM), in the presence (10 μM) or absence of either T140 or Bpa-containing T140 analogs. Cells were then washed, irradiated for 1 h at 4 °C under filtered UV light in washing buffer and centrifuged at 3500 × *g* for 15 min at 4 °C. The pellet was solubilized on ice for 30 min in modified radioimmunoprecipitation buffer [m-RIPA; 50 mM Tris/HCl, pH 7.5, 150 mM NaCl, 5 mM sodium azide, 1% (v/v) nonidet P40, 0.25% (v/v) deoxycholic acid and 0.1% (w/v) SDS] containing complete protease inhibitor cocktail. After centrifugation at 15 000 × *g* for 30 min at 4 °C, the supernatants were kept at −80 °C until further analysis.

2.7. Partial purification of the labeled complex

Photolabeled receptors were separated by SDS-PAGE using 10% (w/v) acrylamide/Tris/glycine gels followed by autoradiography using X-Omat® Blue (XB) films (Kodak). Bands corresponding to ligand-receptor complexes were excised from the gels and submitted to electroelution. Eluted proteins were then concentrated and kept at −80 °C.

2.8. Endoglycosidase and proteolytic digestions of the radiophotolabeled complex

For endoglycosidase digestions, partially purified photolabeled receptors (3500 cpm), were resuspended in 50 μl of digestion buffer (200 mM potassium phosphate buffer pH 7.0, 50 mM EDTA, 0.5% Nonidet P40) and samples were incubated with 5 units of PNGase F for 16 h at room temperature. For V8 protease digestions,

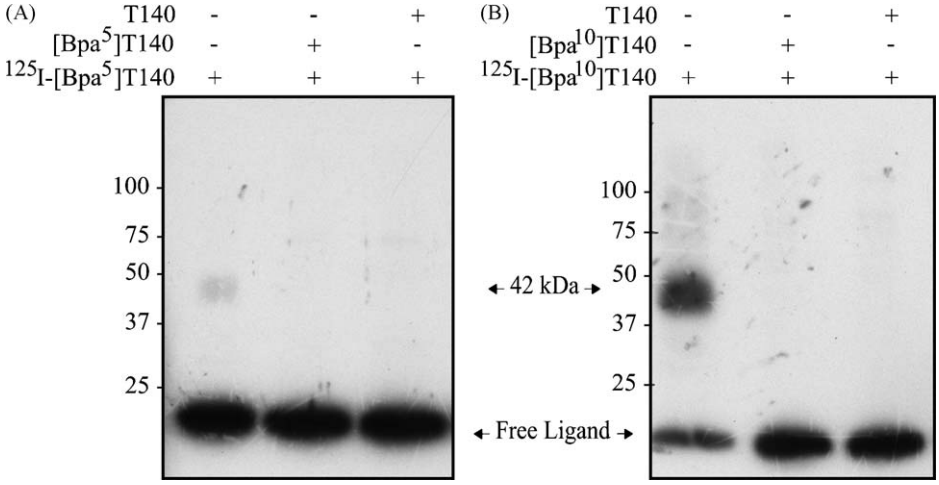

Fig. 4. Photolabeling of CXCR4 in the presence of T140. HEK293 stably expressing CXCR4 were photolabeled using ^{125}I-[Bpa^5]T140 (A). Total labeling (lane 1), labeling in the presence of 10 μM [Bpa^5]T140 (lane 2) and labeling in the presence of 10 μM T140 (lane 3). HEK293 stably expressing CXCR4 were photolabeled using ^{125}I-[Bpa^{10}]T140 (B). Total labeling (lane 1), labeling in the presence of 10 μM [Bpa^{10}]T140 (lane 2) and labeling in the presence of 10 μM T140 (lane 3). After photolabeling, cellular proteins were solubilized, denatured and submitted to SDS-PAGE on 10% acrylamide gel followed by autoradiography. Protein standards of the indicated molecular masses (kDa) are run in parallel. These results are representative of at least 3 separate experiments.

partially purified photolabeled receptors (3500 cpm) were resuspended in 50 μl of digestion buffer (100 mM ammonium bicarbonate buffer, pH 8.0) and incubated with 5 μg of V8 protease at room temperature for 16 h. Under these conditions, V8 protease cleaves at the C-terminal side of glutamate residues. For endo Asp-N digestion, partially purified photolabeled receptors (5000 c.p.m.) were resuspended in 50 μl of digestion buffer (50 mM Na_2HPO_4, pH 7.4, 0.01% SDS), and samples were incubated with endo Asp-N (0.5 μg) for 16 h at room temperature. Under these conditions, endo Asp-N cleaves at the N-terminal side of aspartate residues. When subsequent digestions were needed, products of the first digestion were run on a 16.5% (w/v) acrylamide/Tris/Tricine gel, and the corresponding band was electroeluted. Eluted proteins were concentrated and submitted to subsequent digestion. The products of proteolysis were analyzed by SDS-PAGE using 16.5% (w/v) acrylamide/Tris/Tricine gels, followed by autoradiography on X-ray films (BioMax® MS) with intensifying screens. ^{14}C-labeled low-molecular-mass protein standards (Amersham Biosciences) were used to determine apparent molecular masses.

2.9. Molecular modeling

All calculations were performed on a Silicon Graphics Octane2 workstation (Silicon Graphics Inc. Mountain View, CA, U.S.A.). Molecular modeling of the CXCR4 receptor and T140-CXCR4 receptor complex was done with the INSIGHTII suite of programs (Homology, Discover and Biopolymer; Accelerys, San Diego, CA). The molecular model of human CXCR4 (GenBank™ accession no. **P61073**) was based on the crystal structure of opsin (pdb accession number 3dqb) [37]. The sequence alignment between the CXCR4 receptor and the opsin sequence was used to identify and assign the structurally conserved regions (SCRs). All the strictly conserved residues of family A members were aligned. There were no gaps in any of the TMDs. The coordinates of the assigned SCRs were then transferred to the sequence of CXCR4, followed by the generation of the intra and extracellular loops with the database found in Homology. The potential energy of the model was minimized using Discover as described in [31]; first by fixing all heavy atoms, then by fixing only the backbone and, finally, by fixing the backbone of the TMD. The disulfide bonds (between ECL1 and ECL2 and

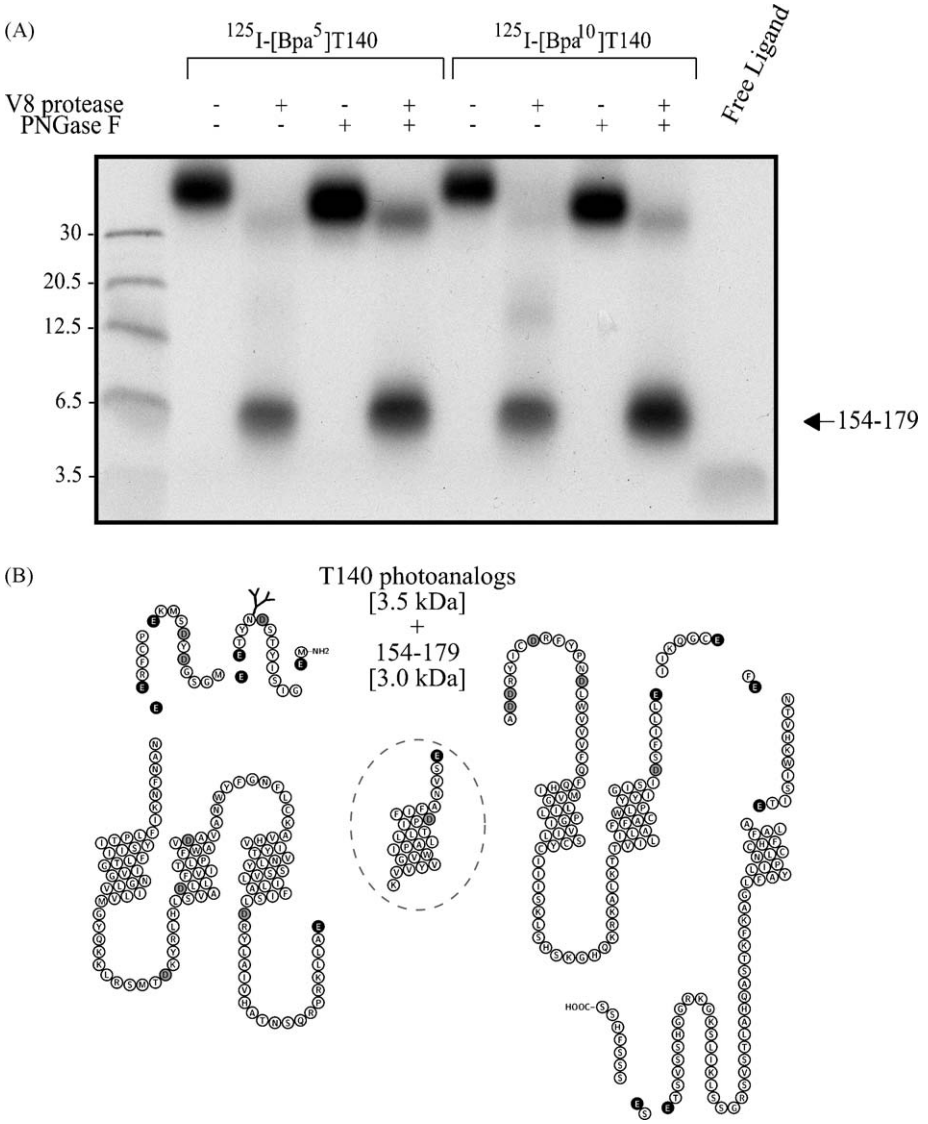

Fig. 5. Proteolytic cleavage of ^{125}I-[Bpa^5]T140 and ^{125}I-[Bpa^{10}]T140 photolabeled CXCR4 with V8 protease. (A) Partially purified photolabeled CXCR4 (3500 cpm) was incubated in absence (lanes 1, 3, 5, 7) or in presence of V8 protease (lanes 2, 4, 6, 8) (5 μg); lanes 1, 2, 5, 6 show glycosylated photolabeled CXCR4; lanes 3, 4, 7, 8 show PNGase treated (deglycosylated) photolabeled CXCR4. Lanes 1–4: ^{125}I-[Bpa^5]T140 photolabeled CXCR4. Lanes 5–8: ^{125}I-[Bpa^{10}]T140 photolabeled CXCR4. Samples were run on a 16.5% Tris/Tricine acrylamide gel followed by autoradiography. ^{14}C-labeled protein standards of the indicated molecular masses (kDa) were run in parallel. These results are representative of at least three separate experiments. (B) Two-dimensional representation of the primary structure of human CXCR4 receptor cleaved by V8 protease.

between N-terminal and ECL3) were then added to CXCR4 and the potential energy was minimized again by fixing all heavy atoms besides the concerned loops and the N-terminus, which were left unrestrained.

2.10. Generation of liganded receptor structures by molecular modeling

The T140 ligand was constructed with INSIGHTII BUILDER based on the reported NMR solution structure of T140 [38] and the molecule was placed in CXCR4's binding pocket with Tyr^5 and Tyr^{10} facing towards TM4, as suggested by the photolabeling results. For the minimization process, CXCR4's TMD were fixed and the T140 ligand was left completely unrestrained. The complex was minimized until the maximum derivative was less than 0.1 kcal/mol.

3. Results

3.1. Binding specificity of the photoreactive analogs

Fig. 1 shows the primary structure of T140 and the photoreactive analogs used in the present study (Fig. 1A) as well as the CXCR4 receptor (Fig. 1B). Tyr^5 and Tyr^{10} were respectively replaced by Bpa to give [Bpa^5]T140 and [Bpa^{10}]T140. We validated our HEK293 cells stably expressing CXCR4 by competition binding assays. Fig. 2A shows that we found a 2.5-fold increase in total specific ^{125}I-SDF-1α binding on HEK293 stably expressing CXCR4 as compared to untransfected HEK293 cells. Binding of SDF-1α to untransfected HEK293 cells is due to the presence of trace endogenous CXCR4 receptors as previously reported [39]. Displacement binding of ^{125}I-SDF-1α with unlabeled SDF-1α showed a dose dependant fit for a two site model ($R^2 = 0.9866$) as previously observed in transfected HEK293T cells [40] and in Jurkat cells endogenously expressing CXCR4 [41]. The SDF-1α high affinity site for CXCR4 has a K_i value of 0.4 ± 0.4 nM, while the low affinity site has a K_i of 31 ± 12 nM (Fig. 2A, Table 1). In competitive binding assays, the photoanalogs [Bpa^5]T140 and [Bpa^{10}]T140 (Fig. 2B) exhibited K_i values of 2.8 ± 0.9 nM and 1.1 ± 0.8 nM respectively for the high affinity site of ^{125}I-SDF-1α on CXCR4 compared to 2.6 ± 2.5 nM for T140. For the low affinity site, [Bpa^5]T140 and [Bpa^{10}]T140 showed K_i values of 40 ± 20 nM and 63 ± 8.8 nM respectively compared to 84 ± 36 nM for T140. Similar K_i values between T140 and the photoanalogs confirmed that substitution of Tyr^5 and Tyr^{10} with Bpa did not alter their affinity for CXCR4.

To assess whether T140 bound CXCR4's orthosteric site, we performed dissociation kinetics experiments using ^{125}I-SDF-1α in absence or presence of 1 μM or 10 μM of T140 (Fig. 2C). Dissociation kinetic measurements are used to detect conformational changes induced by an allosteric compound that usually slows the dissociation of the orthosteric ligand [34]. The dissociation curves revealed no significant changes in the dissociation rate whether T140 was absent ($K = 0.029 \pm 0.0043\ min^{-1}$) or present at either 1 μM ($K = 0.034 \pm 0.0063\ min^{-1}$) or 10 μM ($K = 0.033 \pm 0.011\ min^{-1}$). This suggests that T140 binds within CXCR4's orthosteric binding pocket.

3.2. HIV infection blockade by T140 photoanalogs

To further assess the functionality of the T140 photoanalogs, we determined their potency at inhibiting HIV infection (Table 2). While the observed IC_{50} of T140 in our conditions was 54 nM, similar to previously reported values (26 nM in [19], 90 nM in [42]), both photoanalogs had reduced IC_{50}s of 261 nM and 107 nM for [Bpa^5]T140 and [Bpa^{10}]T140 respectively, maintaining their capacity at blocking HIV infection albeit at lower potencies.

3.3. Photolabeling of human CXCR4 receptor

Since good affinities towards CXCR4 had been observed for both photoanalogs, ^{125}I-[Bpa^5]T140 and ^{125}I-[Bpa^{10}]T140 were subsequently used in photolabeling experiments. When incubated with membranes of HEK293 cells stably expressing CXCR4, both photoanalogs covalently labeled a protein migrating at 42 kDa on SDS-PAGE. However a significantly reduced labeling yield was observed for ^{125}I-[Bpa^5]T140 compared to ^{125}I-[Bpa^{10}]T140 (Fig. 3). This 42 kDa band was not observed in untransfected HEK293 confirming the identity of the labeled protein as CXCR4. Although we did find CXCR4-dependent SDF-1α binding in untransfected cells, it is possible that photolabeling conditions are not as sensitive as γ-radiation counting and do not permit detection of trace endogenous CXCR4. The labeling of CXCR4 by ^{125}I-[Bpa^5]T140 and ^{125}I-[Bpa^{10}]T140 was abolished in presence of [Bpa^5]T140 (10 μM) and [Bpa^{10}]T140 (10 μM) respectively, thereby confirming the specificity of the labeling (Fig. 4). Photolabeling of CXCR4 with both photoanalogs was also abolished in presence of native T140 (10 μM) in agreement with the fact that

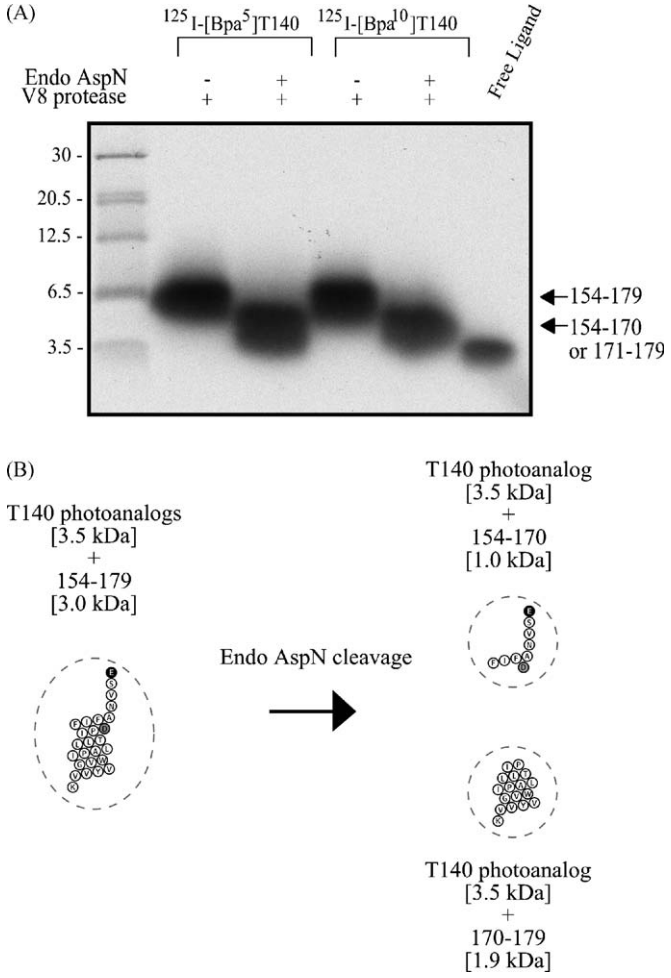

Fig. 6. Proteolytic cleavage of ^{125}I-[Bpa^5]T140 and ^{125}I-[Bpa^{10}]T140 photolabeled fragment Lys^{154}-Glu^{179} of CXCR4 with Endo Asp-N. (A) Partially purified photolabeled fragment Lys^{154}-Glu^{179} of CXCR4 (3500 cpm) was incubated in absence (lanes 1, 3) or in the presence of Endo Asp-N (lanes 2, 4) (5 μg). Lanes 1–2: ^{125}I-[Bpa^5]T140 photolabeled Lys^{154}-Glu^{179} fragment. Lanes 3–4: ^{125}I-[Bpa^{10}]T140 photolabeled fragment Lys^{154}-Glu^{179}. Samples were run on a 16.5% Tris/Tricine acrylamide gel followed by autoradiography. ^{14}C-labeled protein standards of the indicated molecular masses (kDa) were run in parallel. These results are representative of at least three separate experiments. (B) Two-dimensional representation of the Lys^{154}-Glu^{179} fragment of CXCR4 cleaved by Endo Asp-N.

the photoanalogs interact within the same confines of T140's binding pocket.

3.4. V8 protease digestion of ^{125}I-[Bpa^{5}]T140/CXCR4 and ^{125}I-[Bpa^{10}]T140/CXCR4 complexes

To map the ligand–receptor contact site(s), the 42 kDa photoligand–receptor complex was partially purified and submitted to V8 protease digestion which cleaves on the C-terminal side of glutamate residues. This digestion produced a band migrating at 6.5 kDa for both ^{125}I-[Bpa^{5}]T140/CXCR4 and ^{125}I-[Bpa^{10}]T140/CXCR4 complexes. The partially purified complex was also submitted to PNGase F and further treatment with V8 protease also generated a 6.5 kDa band (Fig. 5) suggesting the absence of *N*-glycosylation on this fragment. The only fragment corresponding to this molecular weight was one encompassing Lys^{154}–Glu^{179} of the receptor's fourth transmembrane domain with a calculated mass of 3.0 kDa in addition to the mass of the photoligand (3.5 kDa) as observed on SDS-PAGE gel (Fig. 5).

3.5. Endo AspN protease digestion of fragment Lys^{154}-Glu^{179}

To further refine the binding site(s) of the photoanalogs, we partially purified the Lys^{154}-Glu^{179} fragment obtained previously by V8 protease digestion of the native complex and digested it with endo AspN protease, which cleaves on the N-terminal side of aspartate residues. The Lys^{154}-Glu^{179} fragment has a single Asp residue in its sequence (Asp^{171}), resulting in two possible fragments: Lys^{154}-Pro^{170} (1.9 kDa) and Asp^{171}-Glu^{179} (1.0 kDa). Endo AspN digestion led to the cleavage of the Lys^{154}-Glu^{179} fragment validating that photolabeling site(s) of both photoanalogs occurred in this region of the receptor (Fig. 6). However, the limited resolution of the SDS-PAGE conditions under which we separate the photolabeled fragments did not enable us to delineate whether labeling occurred in a fragment corresponding to residues Lys^{154}-Pro^{170} or Asp^{171}-Glu^{179} for both photoanalogs.

3.6. Molecular modeling of the CXCR4–T140 complex

To extend the analysis of the T140 binding site on CXCR4, we performed molecular modeling using the reported NMR solution structure of T140 [38]. This structure consists of a β-hairpin with a type II′ β-turn with residues Tyr^{5} and Tyr^{10} on the same side of the T140 β-hairpin (see Fig. 7A). Since both photoanalogs labeled the same region of CXCR4 (i.e. the Lys^{154}-Glu^{179} fragment within TM4), it is reasonable to assume that this side of T140 lies in close proximity to the Lys^{154}-Glu^{179} region of the receptor. Whereas our results indicate that both Tyr^{5} and Tyr^{10} can contact residues from Leu^{154} to Glu^{179}, it does not allow us to determine the exact orientation of T140 in the complex. However, considering that

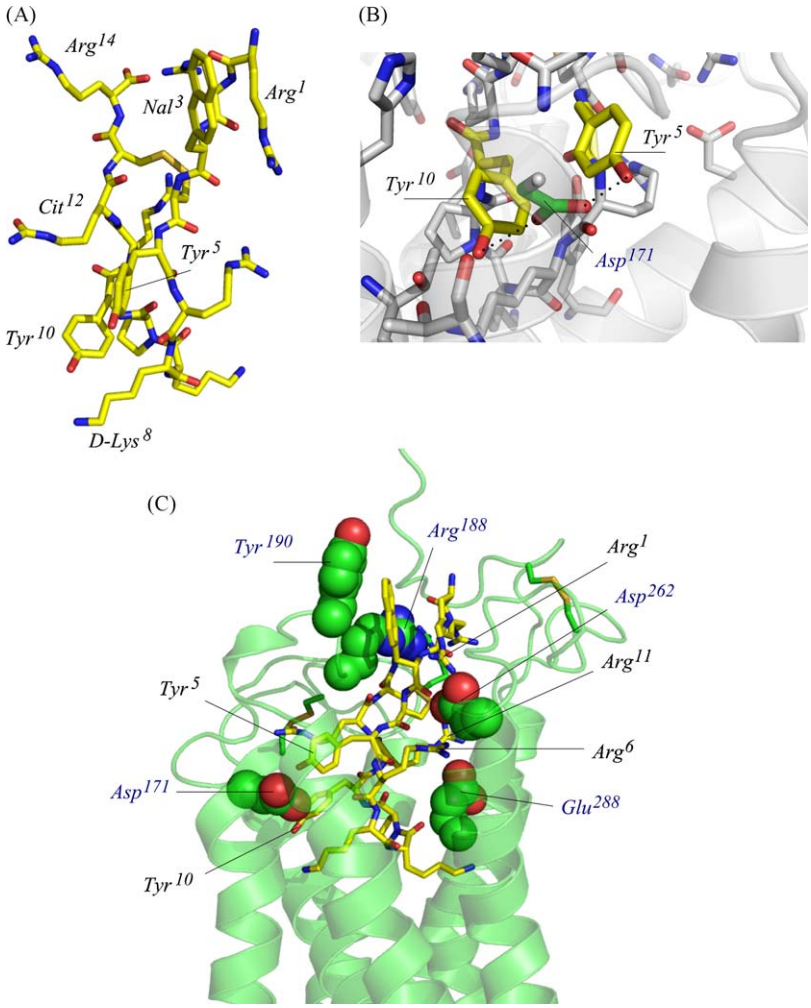

Fig. 7. Molecular model of the T140 liganded CXCR4. (A) NMR structure of T140 [38]. Note that Tyr^{5} and Tyr^{10} are on the same face of the disufide-linked β-hairpin. (B) Tyr^{5} and Tyr^{10} (yellow) of T140 are positioned to form specific H-bonds with Asp^{171} (green) of CXCR4. (C) Global view of the model of the complex between T140 and CXCR4 (green) with an emphasis on key interactions of T140 (indicated in black) with key residues (indicated in blue) on CXCR4. See text for further details.

T140 is positively charged both above and below the disulfide bond, we hypothesized that the N- and C-terminal ends of T140 will be oriented towards the extracellular domains of CXCR4 with the type II′ β-turn buried deep into the binding pocket. Thus, T140 would insert itself in the CXCR4 orthosteric binding pocket as a U-shaped ligand with residues 5 and 10 interacting with TM4.

4. Discussion

The identification of residues involved in formation of a receptor's binding pocket is an important step in understanding the bimolecular recognition between a ligand and its receptor. In this study, we used photoaffinity labeling as a strategy to identify CXCR4 residues found in close proximity to the inverse agonist T140. This approach depends on the spatial proximity between the photoligand and the receptor's residues that are oriented towards the binding pocket in order to form a covalent conjugate that can be further analyzed biochemically for the identification of interaction sites.

Previous reports on the structure–activity of T140 had shown that replacing either Arg^{2}, Nal^{3}, Tyr^{5} and Arg^{14} with alanine caused a significant decrease in the anti-HIV activity of T140 [23]. However, the overall binding properties of these analogs on CXCR4 had not been assessed. To facilitate production of photoanalogs incorporating a radioactive, iodinated Tyr residue, we substituted either Tyr at position 5 or position 10 of the original T140 sequence with the photoreactive Bpa amino acid. The resulting T140 photoligands as well as T140 and SDF-1α presented high affinities (Table 1) for the orthosteric pocket of the CXCR4 receptor as defined by binding and dissociation kinetic experiments. T140 and the photoanalogs also exhibited antiviral activity in HIV-1 infection assays. These results suggest that the Bpa substitutions of Tyr^{5} and Tyr^{10} did not alter the properties of native T140, making them functional candidates for the identification of the T140 binding pocket on CXCR4.

We further characterized these peptides for their ability to recognize and to label the CXCR4 receptor. ^{125}I-[Bpa^{5}]T140 and ^{125}I-[Bpa^{10}]T140 both labeled CXCR4 and the resulting complex migrates at 42 kDa. ^{125}I-[Bpa^{5}]T140 showed reduced labeling of CXCR4 compared to ^{125}I-[Bpa^{10}]T140 although both analogs exhibited similar affinities. The reduced CXCR4 labeling by ^{125}I-[Bpa^{5}]T140 compared to ^{125}I-[Bpa^{10}]T140 is due to the photolabeling reaction that is itself highly dependent on the proximity of residues surrounding Bpa which may influence the photolabeling yield. Residues influencing the photolabeling yield of a receptor without affecting the affinity of the photoanalog have been demonstrated for other receptors [43].

Labeling of CXCR4 by ^{125}I-[Bpa^{5}]T140 and ^{125}I-[Bpa^{10}]T140 was completely abolished by the presence of unlabeled photoanalogs and with native T140 suggesting that the photoanalogs are specific for the T140 binding site. Using PNGase F and V8 protease digestions, a 6.5 kDa fragment corresponding to Asn^{154}–Glu^{179} was labeled with either ^{125}I-[Bpa^{5}]T140 or ^{125}I-[Bpa^{10}]T140. Further digestion of this fragment with endo Asp-N, cleaved at Asp^{171} thereby confirming that both T140 photoanalogs were labeling this region. This suggests that specific TM4 residues of CXCR4 are in close proximity to residues 5 and 10 of T140.

Using site-directed mutagenesis, the potential involvement of CXCR4's TM4 in T140 binding and in mediating human immunodeficiency virus entry have been reported [27]. Substituting Asp^{171} of TM4 as well as Arg^{188} and Tyr^{190} of ECL2 for alanine led to a loss of sensitivity to T140 inhibition of Env-mediated fusion. Binding experiments confirmed that these residues were critical for T140 binding to CXCR4. Using these results to perform molecular modeling it was suggested that the N-terminus of T140 interacted with ECL2 of CXCR4 while the C-terminus was interacting with TM4, ECL2 and ECL3. The authors proposed that Arg^{14} of T140 forms a hydrogen bond with Asp^{171} of CXCR4, while Phe^{174}, Arg^{188}, Tyr^{190} and Phe^{201} of CXCR4 are involved in a hydrophobic network with Nal^{3} and Tyr^{5} of T140. This led to a model in which the two beta strands of T140 positioned perpendicular to the TMs, with the N-terminal strand lying on top of the C-terminal strand and with the type II′ β-turn extending away from the binding pocket.

In our model, we find that restraining the position of Tyr^{5} and Tyr^{10} of T140 close to residues Leu^{154} to Glu^{179} of CXCR4 during the potential energy minimization leads to the formation of H-bonds (internal solvation) between the two side-chain $^{\eta}$OH and the carboxylate of Asp^{171} (Fig. 7B). This locks the two beta strands of T140 parallel to the TMs. In addition, we find that Arg^{1}, Arg^{6} and Arg^{11} of T140 forms an extensive number of favorable electrostatic interactions and H-bonds with two other conserved negatively charged side-chains, Asp^{262} and Glu^{288} (Fig. 7C and Table S1 in supplementary material). This is in agreement with a thermodynamically stable configuration of this complex. Moreover, Asp^{171}, Asp^{262} and Glu^{288} have been identified as key residues in CXCR4 co-receptor function in HIV-1 entry [24]. Hence, these results support the notion that these interactions are critical for the formation of a stable complex between CXCR4 and T140. Similarly to the model proposed by Trent et al. [27], contact sites between T140 and CXCR4 that we experimentally determined lead to a model where Tyr^{190} is involved in a hydrophobic network with Nal^{3}. Note that Arg^{188} is also part of this hydrophobic network through its methylenes and forms a salt-bridge with the terminal carboxylate of T140. We also observe the existence of a network of additional solvent exposed salt bridges between negatively charged side-chains of acidic residues found in ECL2 and Arg^{1} and Arg^{14} of T140 (see Fig. 7C and Table S1 in supplementary material). In summary, we find that the complex between T140 and CXCR4 depicts an optimized array of electrostatic interactions and H-Bonds. Such an array of interactions is the hallmark of molecular recognition. Finally, it is noteworthy that the residues on CXCR4 found to be critical for T140 inhibition of Env-mediated fusion are involved in an array of specific interactions in our model. Knowingly, it can be argued that this functional analysis of the T140-CXCR4 interactions adequately supports our model based on direct contacts obtained by photolabeling.

In conclusion, our results offer a novel view and interpretation of the T140 binding site and its interactions with CXCR4. Indeed, using photoaffinity labeling, we demonstrate interaction of Tyr^{5} and Tyr^{10} of T140 with a precise domain in TM4 of CXCR4. Our overall view of this interaction takes the form of a U-shaped T140 ligand inserting itself deeper in CXCR4's binding pocket than previous models depicted, suggesting a new interpretation of the key residues involved in the binding of anti-HIV compounds like T140.

Acknowledgements

We thank Michel Bouvier (Department of Biochemistry, Institute for Research in Immunology and Cancer, Université de Montréal, Montréal, Québec, Canada) for the HEK293-CXCR4 stable cell line and Marie-Reine Lefebvre (Department of Pharmacology, Université de Sherbrooke, Sherbrooke, Québec, Canada) for the synthesis of T140 and T140 photoanalogs. We also thank Brian J. Holleran for critical reading of the manuscript. This work was supported by a grant from the Canadian Institutes for Health Research (CIHR) Team in GPCR Allosteric Regulation (CTiGAR) and is part of the Ph.D. thesis of P.E.B. D.D. holds a CIHR postdoctoral fellowship. E.E. is the recipient of the J.C. Edwards Chair in cardiovascular research. P.L. is a Chercheur boursier senior of the Fonds de la Recherche en Santé du Québec (FRSQ). N.H. is a CIHR New Investigator. R.L is a Chercheur National of the FRSQ.

Appendix A. Supplementary data

Supplementary data associated with this article can be found, in the online version, at doi:10.1016/j.bcp.2009.07.007.

References

[1] Baggiolini M. Chemokines and leukocyte traffic. Nature 1998;392:565–8.
[2] Aiuti A, Webb IJ, Bleul C, Springer T, Gutierrez-Ramos JC. The chemokine SDF-1 is a chemoattractant for human CD34+ hematopoietic progenitor cells and provides a new mechanism to explain the mobilization of CD34+ progenitors to peripheral blood. J Exp Med 1997;185:111–20.
[3] Murphy PM, Baggiolini M, Charo IF, Hebert CA, Horuk R, Matsushima K, et al. International union of pharmacology. XXII. Nomenclature for chemokine receptors. Pharmacol Rev 2000;52:145–76.
[4] Broxmeyer HE. Chemokines in hematopoiesis. Curr Opin Hematol 2008;15:49–58.
[5] Chute JP. Stem cell homing. Curr Opin Hematol 2006;13:399–406.
[6] Salcedo R, Oppenheim JJ. Role of chemokines in angiogenesis: CXCL12/SDF-1 and CXCR4 interaction, a key regulator of endothelial cell responses. Microcirculation 2003;10:359–70.
[7] Iwamoto T, Okamoto H, Toyama Y, Momohara S. Molecular aspects of rheumatoid arthritis: chemokines in the joints of patients. FEBS J 2008;275:4448–55.
[8] Vandercappellen J, Van Damme J, Struyf S. The role of CXC chemokines and their receptors in cancer. Cancer Lett 2008;267:226–44.
[9] Oberlin E, Amara A, Bachelerie F, Bessia C, Virelizier JL, Arenzana-Seisdedos F, et al. The CXC chemokine SDF-1 is the ligand for LESTR/fusin and prevents infection by T-cell-line-adapted HIV-1. Nature 1996;382:833–5.
[10] Balabanian K, Lagane B, Infantino S, Chow KY, Harriague J, Moepps B, et al. The chemokine SDF-1/CXCL12 binds to and signals through the orphan receptor RDC1 in T lymphocytes. J Biol Chem 2005;280:35760–6.
[11] Suratt BT, Petty JM, Young SK, Malcolm KC, Lieber JG, Nick JA, et al. Role of the CXCR4/SDF-1 chemokine axis in circulating neutrophil homeostasis. Blood 2004;104:565–71.
[12] Benovic JL, Marchese A. A new key in breast cancer metastasis. Cancer Cell 2004;6:429–30.
[13] Raman D, Baugher PJ, Thu YM, Richmond A. Role of chemokines in tumor growth. Cancer Lett 2007;256:137–65.
[14] Feng Y, Broder CC, Kennedy PE, Berger EA. HIV-1 entry cofactor: functional cDNA cloning of a seven-transmembrane, G protein-coupled receptor. Science 1996;272:872–7.
[15] Lusso P. HIV and the chemokine system: 10 years later. EMBO J 2006;25:447–56.
[16] Donzella GA, Schols D, Lin SW, Este JA, Nagashima KA, Maddon PJ, et al. AMD3100, a small molecule inhibitor of HIV-1 entry via the CXCR4 co-receptor. Nat Med 1998;4:72–7.
[17] Tamamura H, Xu Y, Hattori T, Zhang X, Arakaki R, Kanbara K, et al. A low-molecular-weight inhibitor against the chemokine receptor CXCR4: a strong anti-HIV peptide T140. Biochem Biophys Res Commun 1998;253:877–82.
[18] Fujii N, Tamamura H. Peptide-lead CXCR4 antagonists with high anti-HIV activity. Curr Opin Investig Drugs 2001;2:1198–202.
[19] Tamamura H, Tsutsumi H, Masuno H, Mizokami S, Hiramatsu K, Wang Z, et al. Development of a linear type of low molecular weight CXCR4 antagonists based on T140 analogs. Org Biomol Chem 2006;4:2354–7.
[20] Tamamura H, Fujisawa M, Hiramatsu K, Mizumoto M, Nakashima H, Yamamoto N, et al. Identification of a CXCR4 antagonist, a T140 analog, as an anti-rheumatoid arthritis agent. FEBS Lett 2004;569:99–104.
[21] Tamamura H, Hori A, Kanzaki N, Hiramatsu K, Mizumoto M, Nakashima H, et al. T140 analogs as CXCR4 antagonists identified as anti-metastatic agents in the treatment of breast cancer. FEBS Lett 2003;550:79–83.
[22] Zhang WB, Navenot JM, Haribabu B, Tamamura H, Hiramatu K, Omagari A, et al. A point mutation that confers constitutive activity to CXCR4 reveals that T140 is an inverse agonist and that AMD3100 and ALX40-4C are weak partial agonists. J Biol Chem 2002;277:24515–21.
[23] Tamamura H, Omagari A, Oishi S, Kanamoto T, Yamamoto N, Peiper SC, et al. Pharmacophore identification of a specific CXCR4 inhibitor, T140, leads to development of effective anti-HIV agents with very high selectivity indexes. Bioorg Med Chem Lett 2000;10:2633–7.
[24] Brelot A, Heveker N, Montes M, Alizon M. Identification of residues of CXCR4 critical for human immunodeficiency virus coreceptor and chemokine receptor activities. J Biol Chem 2000;275:23736–44.
[25] Zhou N, Luo Z, Luo J, Liu D, Hall JW, Pomerantz RJ, et al. Structural and functional characterization of human CXCR4 as a chemokine receptor and HIV-1 co-receptor by mutagenesis and molecular modeling studies. J Biol Chem 2001;276:42826–33.
[26] Basmaciogullari S, Babcock GJ, Van Ryk D, Wojtowicz W, Sodroski J. Identification of conserved and variable structures in the human immunodeficiency virus gp120 glycoprotein of importance for CXCR4 binding. J Virol 2002;76:10791–800.
[27] Trent JO, Wang ZX, Murray JL, Shao W, Tamamura H, Fujii N, et al. Lipid bilayer simulations of CXCR4 with inverse agonists and weak partial agonists. J Biol Chem 2003;278:47136–44.
[28] Dorman G, Prestwich GD. Benzophenone photophores in biochemistry. Biochemistry 1994;33:5661–73.
[29] Boucard AA, Wilkes BC, Laporte SA, Escher E, Guillemette G, Leduc R. Photolabeling identifies position 172 of the human AT(1) receptor as a ligand contact point: receptor-bound angiotensin II adopts an extended structure. Biochemistry 2000;39:9662–70.
[30] Laporte SA, Boucard AA, Servant G, Guillemette G, Leduc R, Escher E. Determination of peptide contact points in the human angiotensin II type I receptor (AT1) with photosensitive analogs of angiotensin II. Mol Endocrinol 1999;13:578–86.
[31] Holleran BJ, Beaulieu ME, Proulx CD, Lavigne P, Escher E, Leduc R. Photolabelling the urotensin II receptor reveals distinct agonist- and partial-agonist-binding sites. Biochem J 2007;402:51–61.
[32] Coulie B, Matsuura B, Dong M, Hadac EM, Pinon DI, Feighner SD, et al. Identification of peptide ligand-binding domains within the human motilin receptor using photoaffinity labeling. J Biol Chem 2001;276:35518–22.
[33] Fraker PJ, Speck Jr JC. Protein and cell membrane iodinations with a sparingly soluble chloroamide, 1,3,4,6-tetrachloro-3a,6a-diphrenylglycoluril. Biochem Biophys Res Commun 1978;80:849–57.
[34] Price MR, Baillie GL, Thomas A, Stevenson LA, Easson M, Goodwin R, et al. Allosteric modulation of the cannabinoid CB1 receptor. Mol Pharmacol 2005;68:1484–95.
[35] Munch J, Standker L, Pohlmann S, Baribaud F, Papkalla A, Rosorius O, et al. Hemofiltrate CC chemokine 1[9-74] causes effective internalization of CCR5 and is a potent inhibitor of R5-tropic human immunodeficiency virus type 1 strains in primary T cells and macrophages. Antimicrob Agents Chemother 2002;46:982–90.
[36] Collman R, Balliet JW, Gregory SA, Friedman H, Kolson DL, Nathanson N, et al. An infectious molecular clone of an unusual macrophage-tropic and highly cytopathic strain of human immunodeficiency virus type 1. J Virol 1992;66:7517–21.
[37] Scheerer P, Park JH, Hildebrand PW, Kim YJ, Krauss N, Choe HW, et al. Crystal structure of opsin in its G-protein-interacting conformation. Nature 2008;455:497–502.
[38] Tamamura H, Sugioka M, Odagaki Y, Omagari A, Kan Y, Oishi S, et al. Conformational study of a highly specific CXCR4 inhibitor, T140, disclosing the close proximity of its intrinsic pharmacophores associated with strong anti-HIV activity. Bioorg Med Chem Lett 2001;11:359–62.
[39] Sierro F, Biben C, Martinez-Munoz L, Mellado M, Ransohoff RM, Li M, et al. Disrupted cardiac development but normal hematopoiesis in mice deficient in the second CXCL12/SDF-1 receptor, CXCR7. Proc Natl Acad Sci USA 2007;104:14759–64.
[40] Kalatskaya I, Berchiche YA, Gravel S, Limberg BJ, Rosenbaum JS, Heveker N. AMD3100 is a CXCR7 ligand with allosteric agonist properties. Mol Pharmacol 2009;75:1240–7.
[41] Gupta SK, Pillarisetti K, Thomas RA, Aiyar N. Pharmacological evidence for complex and multiple site interaction of CXCR4 with SDF-1alpha: implications for development of selective CXCR4 antagonists. Immunol Lett 2001;78:29–34.
[42] Lin G, Bertolotti-Ciarlet A, Haggarty B, Romano J, Nolan KM, Leslie GJ, et al. Replication-competent variants of human immunodeficiency virus type 2 lacking the V3 loop exhibit resistance to chemokine receptor antagonists. J Virol 2007;81:9956–66.
[43] Fillion D, Deraet M, Holleran BJ, Escher E. Stereospecific synthesis of a carbene-generating angiotensin II analogue for comparative photoaffinity labeling: improved incorporation and absence of methionine selectivity. J Med Chem 2006;49:2200–9.